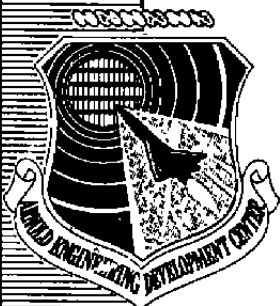


*To Doctor For  
Alas! I knew him before  
RJR*



# INVESTIGATION OF SUBSONIC ANNULAR NOZZLES FOR ENGINE EXHAUST/EXTERNAL FLOW INTERACTION STUDIES

ENGINE TEST FACILITY  
ARNOLD ENGINEERING DEVELOPMENT CENTER  
AIR FORCE SYSTEMS COMMAND  
ARNOLD AIR FORCE STATION, TENNESSEE 37389

December 1976

Final Report for Period August 1973 — June 1976

Approved for public release; distribution unlimited.

Prepared for

DIRECTORATE OF TECHNOLOGY (DY)  
ARNOLD ENGINEERING DEVELOPMENT CENTER  
ARNOLD AIR FORCE STATION, TENNESSEE 37389

## NOTICES

When U. S. Government drawings specifications, or other data are used for any purpose other than a definitely related Government procurement operation, the Government thereby incurs no responsibility nor any obligation whatsoever, and the fact that the Government may have formulated, furnished, or in any way supplied the said drawings, specifications, or other data, is not to be regarded by implication or otherwise, or in any manner licensing the holder or any other person or corporation, or conveying any rights or permission to manufacture, use, or sell any patented invention that may in any way be related thereto.

Qualified users may obtain copies of this report from the Defense Documentation Center.

References to named commercial products in this report are not to be considered in any sense as an endorsement of the product by the United States Air Force or the Government.

This report has been reviewed by the Information Office (OI) and is releasable to the National Technical Information Service (NTIS). At NTIS, it will be available to the general public, including foreign nations.

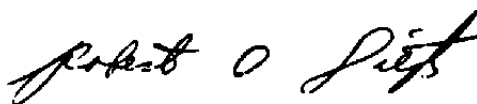
## APPROVAL STATEMENT

This technical report has been reviewed and is approved for publication.

FOR THE COMMANDER



ELTON R. THOMPSON  
Research & Development  
Division  
Directorate of Technology



ROBERT O. DIETZ  
Director of Technology

**UNCLASSIFIED**

DD FORM 1473 EDITION OF 1 NOV 65 IS OBSOLETE

**UNCLASSIFIED**

# UNCLASSIFIED

## 20. ABSTRACT (Continued)

distributions and boattail pressure drag coefficients obtained on the afterbody in the annular jet were compared with wind tunnel results obtained with boattail approach Mach numbers between 0.5 and 1.0. Boundary-layer profiles were also obtained during the wind tunnel and the annular jet tests. These data are presented and discussed. While the data obtained on the afterbody in the annular jet show larger aerodynamic interference effects than are desirable, the results indicate that the annular jet test technique may have potential application for engine/external flow interaction studies.

## PREFACE

The work reported herein was conducted by the Arnold Engineering Development Center (AEDC), Air Force Systems Command (AFSC) under Program Element 65807F. The experimental annular jet results were obtained by ARO, Inc. (a subsidiary of Sverdrup Corporation), contract operator of AEDC, AFSC, Arnold Air Force Station, Tennessee. The tests were conducted from August 10, 1973, through June 14, 1974 under ARO Project No. RF412. Analysis and reporting was accomplished from April to June 1976 under ARO Project No. R33A-02A. The author of this report was R. J. Matz, ARO, Inc. The manuscript (ARO Control Number ARO-ETF-TR-76-93) was submitted for publication on August 19, 1976.

The efforts of B. Lubarsky, V. L. Head, and B. J. Blaha, Lewis Research Center, National Aeronautics and Space Administration, who provided the afterbody model and wind tunnel test data noted herein, are gratefully acknowledged.

## CONTENTS

	<u>Page</u>
1.0 INTRODUCTION . . . . .	5
2.0 APPARATUS AND PROCEDURES	
2.1 Afterbody Model . . . . .	6
2.2 Wind Tunnel Tests . . . . .	6
2.3 Annular Jet Tests . . . . .	7
3.0 RESULTS AND DISCUSSION	
3.1 Boundary-Layer Conditions . . . . .	10
3.2 Afterbody Flow Conditions . . . . .	11
3.3 Implication of the Results with Respect to Engine Testing . . . . .	12
4.0 CONCLUSIONS . . . . .	13
REFERENCES . . . . .	14

## ILLUSTRATIONS

### Figure

1. Typical Turbine Engine Exhaust Nozzle Configurations . . . . .	17
2. Annular Jet Test Installations for Missile Model Base Flow Investigations . . . . .	18
3. Subsonic Annular Jet Tunnel for Afterbody Model Investigations (From Ref. 7) . . . . .	20
4. Details of the Afterbody Model . . . . .	21
5. Wind Tunnel Installation (Ref. 8) . . . . .	22
6. Annular Jet Installation . . . . .	23
7. Annular Jet Instrumentation . . . . .	24
8. Variation of Local Afterbody Pressures Obtained in the Wind Tunnel with the Reference Pressure . . . . .	28
9. Typical Static Pressure Distributions Obtained in the Annular Jet Installations . . . . .	29
10. Typical Annular Jet Nozzle Exit Boundary-Layer Velocity Profiles . . . . .	30
11. Comparison of Afterbody Boundary Layers Obtained in the Wind Tunnel and in the Annular Tunnels with Natural Development . . . . .	31
12. Comparison of Afterbody Boundary Layers Obtained in the Wind Tunnel and in the Annular Tunnels with the Roughness Element Installed . . . . .	32
13. Comparison of Boundary-Layer Velocity Profiles Obtained in the Annular Jets with Power Law Representations . . . . .	33
14. Afterbody Mach Number Distributions Obtained with the Short Wind Tunnel Model . . . . .	34

<u>Figure</u>	<u>Page</u>
15. Typical Afterbody Mach Number Distributions Obtained in the 6-in. Annular Tunnel . . . . .	35
16. Deviation of Afterbody Mach Number Distributions Obtained in the Annular Jet Nozzles with Surface Roughness from Wind Tunnel Results . . . . .	36
17. Deviation of Boattail Pressure Drag Coefficients Obtained in the Annular Jet Streams from the Wind Tunnel Results . . . . .	37

**TABLE**

1. Estimated Uncertainty in the Principal Annular Nozzle Test Parameters . . . . .	38
NOMENCLATURE . . . . .	39

## 1.0 INTRODUCTION

Turbine engines equipped with variable-area exhaust nozzles are required in high performance aircraft to achieve efficient operation over a wide range of flight conditions. Exhaust nozzle area variability can be achieved by mechanical, aerodynamic, or combined mechanical and aerodynamic means (Ref. 1). If aerodynamic variability is utilized, as in the case of blow-in-door ejector (BIDE) or plug nozzles (Fig. 1), nozzle performance characteristics are closely coupled to external flow conditions. Since satisfactory theoretical models which include external flow interaction effects are not available (Ref. 2), representative performance characteristics of aerodynamically variable exhaust nozzles must be obtained experimentally.

In the past, satisfactory turbine engine exhaust nozzle performance data has been obtained from static subscale cold-flow model tests (e.g., Ref. 1). However, the nozzles involved were conventional convergent or convergent-divergent configurations in which external flow interactions are manifested only through the impressed static pressure at the nozzle exit plane. With such limited external flow coupling and with the relatively uniform tailpipe flow conditions found in turbojet engines, exhaust nozzle performance was adequately described by static, cold-flow model test results. However, recent studies (Ref. 3) indicate that, in mixed-flow turboprops, tailpipe flow distortions resulting from incomplete mixing of the fan and turbine exhaust streams can lead to nozzle thrust and discharge coefficients that differ from cold-flow model results by as much as 3 to 5 percent. Therefore, even with exhaust nozzles that are relatively insensitive to external flow effects, turboprop tailpipe conditions must be duplicated in development and performance tests to obtain realistic nozzle performance data. Considering all these factors, representative aerodynamically variable exhaust nozzle tests may be obtainable only with the engine installed in a test unit that also provides reasonable external flow simulation. Wind tunnel tests might be considered, but installation of full-scale engines in even the largest propulsion wind tunnels would in some cases result in undesirably high tunnel blockage ratios and installation lengths. A possible alternative to the conventional wind tunnel testing is the annular jet test technique (Ref. 4) which has been employed at the Arnold Engineering Development Center (AEDC) to evaluate relatively large missile base flow models with subsonic (Ref. 5) and supersonic (Ref. 6) external flow conditions. A test installation for the missile base flow experiments is shown in Fig. 2.

A similar free-jet test technique (Fig. 3) has also been used (Ref. 7) to investigate the effects of jet plume shape and entrainment on boattail pressure drag at free-stream Mach numbers between 0.55 and 0.85. Afterbody pressure coefficients obtained from the 8.25-percent blockage ratio\* model were shown to be within  $\pm 0.005$  of results obtained on

---

\*Ratio of the model projected area to the annular nozzle exit area.



a similar afterbody that was evaluated in a porous wall tunnel where the model blockage ratio was 0.18 percent.

The possibility of accomplishing full-scale engine exhaust nozzle/external stream interaction tests with the annular jet test technique in an engine test facility will depend primarily on the maximum flow rates necessary to produce acceptable external flow simulation. Existing and proposed engine test facilities are only capable of providing conditioned air for external flow simulation equal to one-to-two times the flow rates of large proposed turbine engines. With this limitation, annular jet-to-engine diameter ratios could be significantly less than the 2.6 to 3.0 ratios that existed in the previously noted missile afterbody model tests. The present investigations were, therefore, undertaken to obtain some quantification of annular tunnel interference effects to determine whether or not the technique warrants further consideration for engine/external stream interaction studies.

The objective of the studies discussed herein is to experimentally determine the influence of annular jet size on afterbody pressure measurements at subsonic flow conditions. Investigations were limited to external stream Mach numbers from 0.5 to 1.0, where the external stream mass flux in the annular jet test installation is a maximum. A representative engine afterbody model, instrumented with static pressure orifices and a boundary-layer rake, was tested in a relatively large porous wall wind tunnel (Ref. 8) to provide data considered to be aerodynamically interference free. Data on the same afterbody model were then obtained in three annular jet subsonic nozzles which had exit diameters of 1.5, 2.0, and 3.0 times the maximum afterbody diameter. Differences between data obtained in the annular jet tests and the porous wall wind tunnel tests were assumed to be indicative of annular jet interference effects.

## **2.0 APPARATUS AND PROCEDURES**

### **2.1 AFTERBODY MODEL**

The afterbody model tested (Fig. 4) has a 15-deg boattail joined to the shoulder of the 4-in.-diam forebody by a 4-in. radius of curvature fairing. The afterbody is instrumented with static pressure orifices at various axial and radial positions. The pressure measurement used to determine a reference Mach number for the afterbody approach flow is located 1.014 in. downstream (Fig. 4) of the juncture between the forebody and the afterbody model.

### **2.2 WIND TUNNEL TESTS**

The afterbody model was tested with two cone-cylinder forebodies having length-to-diameter ratios of 8.8 and 13.8; respectively, and a 2.68-in.-diam solid body

exhaust jet plume simulator. The model was sting-mounted (Fig. 5) in the NASA, Lewis Research Center, 8- by 6-ft supersonic wind tunnel and tested with 3.1-percent tunnel wall porosity as reported in Ref. 8.

Seventy-four pressures were measured at various locations on the afterbody. Pressures were also measured at 2-in. intervals along the cylindrical forebody. Boundary-layer profiles were measured with an eight-probe rake located 1.0 in. upstream of the forebody-afterbody juncture point. Details of the instrumentation and procedures applicable to the wind tunnel tests may be found in Ref. 8.

## **2.3 ANNULAR JET TESTS**

### **2.3.1 Installation**

The same afterbody model (Fig. 4) used in the wind tunnel tests was installed and tested in an annular jet installation (Fig. 6) in the AEDC Engine Test Facility (ETF) Propulsion Research Cell (R-2A). The afterbody model was mounted on a screw-actuated centerbody assembly that could be translated axially with a chain-drive system. The centerbody was prevented from rotating during the repositioning process by a key in the downstream centerbody support strut. The centerbody diameter was 4.0 in. upstream and 2.68 in. downstream of the afterbody model to duplicate the forebody and plume simulator used in the wind tunnel tests. The centerbody axis was concentric with the annular nozzle axis to within 0.1 in.

Geometrically similar nozzles with throat diameters of 6, 8, and 12 in. were used to produce subsonic external flow conditions over the afterbody. The nozzle contraction sections corresponded to the ASME long radius, low beta series, flow nozzle configuration (Ref. 9). The minimum nozzle size selected was large enough to ensure that the mixing layer developing along the annular jet boundary would not merge with the centerbody boundary layer in the vicinity of the afterbody model. The maximum nozzle size was dictated by the air supply capacity to the R-2A test cell.

A porous plate assembly and two screens (Fig. 6) were installed in the 36-in.-diam inlet plenum to provide uniform flow conditions into the annular jet nozzles. A removable roughness element, formed from woven wire cloth, was installed during some tests in an attempt to produce afterbody boundary-layer conditions in the annular jet tests similar to the boundary layers encountered in the wind tunnel tests.

### 2.3.2 Instrumentation

Instrumentation regions are indicated in Fig. 7. Boundary-layer pressure profiles approaching the afterbody model (Fig. 7d, Region F,  $X_c = -2.0$  in.) and static pressures on the afterbody model (Fig. 7d, Region M) were of principal interest because they could be compared directly with the wind tunnel results. Static pressures were also measured on the forebody and sting (Fig. 7d, Regions F and S) and the annular jet nozzle (Fig. 7c, Region N). Total pressure rakes on the forebody and at the annular jet nozzle exit (Fig. 7c, Region N) were rotated to minimize possible interference with static pressure orifices on the afterbody model.

Pressures were measured with strain-gage transducers which were calibrated in-place before and after each test period. Pressures applied to the transducers during the calibration process were measured with a high-precision, multiple-turn, fused-quartz bourdon tube equipped with a servocontrolled optical transducer that is periodically calibrated against standards traceable to the National Bureau of Standards (NBS). Pressure data were recorded on magnetic tape through the use of multiplexing valves and an automated, sequentially sampling, millivolt-to-digital data acquisition system scanning at a rate of two parameters per second.

Centerbody axial position was determined with a calibrated mechanical revolution counter on the centerbody chain drive sprocket. Air temperature in the inlet plenum was sensed with self-aspirating copper-constantan thermocouples that were monitored with D'Arsonval-type pyrometers.

### 2.3.3 Test Procedures

All annular jet data were obtained at steady-state conditions with the inlet plenum pressure between 12 and 14 psia and inlet temperatures from 40 to 80°F. Annular jet unit Reynolds number was varied from  $2.7 \times 10^6$  to  $4.6 \times 10^6$  per foot as compared to the  $3.6 \times 10^6$  to  $4.6 \times 10^6$  per foot range of the wind tunnel tests.

After annular jet inlet conditions were established, test cell pressure was set to provide the reference afterbody Mach number desired to approximate a wind tunnel test condition. The centerbody was then repositioned with respect to the annular nozzle exit in 1- to 2-in. increments to (1) provide a range of afterbody boundary-layer thicknesses at each reference Mach number, and (2) to determine the effect of axial pressure gradients in the annular jets on afterbody Mach numbers. Reference Mach numbers were varied from 0.48 to 0.98 during the annular jet tests. Centerbody translation from 0 to 7 in. downstream of the annular jet nozzle exit plane produced maximum reference Mach number variations of  $\pm 0.02$ .

### 2.3.4 Data Reduction and Correlation Procedures

Boundary-layer velocity distributions were determined from total pressure rakes and local surface pressure measurements with the assumption that the static pressure is constant through the boundary layer. Local Mach numbers over the afterbody surface were determined from measured afterbody static pressures and the free-stream total pressure obtained from the outermost probes of the forebody boundary-layer rake. The reference Mach number ( $M_{ref}$ ) used to correlate the annular jet and wind tunnel results was based on the pressure measured at the upstream-most pressure orifice on the afterbody (Fig. 4).

Afterbody pressures measured at the 90-deg angular position (see Region M, Fig. 7d) with the wind tunnel model at zero angle of attack were used to obtain local Mach numbers and boattail pressure drag coefficients for comparison with the annular jet tests results. To minimize the uncertainty introduced by slight variations in test conditions, the wind tunnel results for each orifice were interpolated to the reference Mach number of the annular tests. The variation of a given pressure is generally well behaved for reference Mach numbers less than 0.95 as shown in Fig. 8. No corrections for wall interference effects were applied to the wind tunnel data.

Annular jet tunnel interference effects are implied from local Mach number and the boattail pressure force comparisons. Local Mach number computed from pressures obtained at the same afterbody orifice were compared for the same reference Mach number in both the annular jet and the wind tunnel tests. Deviations of local Mach numbers obtained in the annular nozzle tests are expressed as a percentage of the corresponding local Mach number obtained from the wind tunnel data, i.e., for

$$M_{ref_w} = M_{ref_A}$$

then

$$\Delta M_{x_c} \text{ (percent)} = \left( \frac{M_A - M_w}{M_w} \right)_{x_c} \times 100 \text{ percent}$$

Boattail pressure drag coefficient was computed from

$$C_{DB} = \left[ \frac{(4)^2 \cdot (2.68)^2}{(4)^2} \right] \frac{\left[ P_{ref} \cdot \sum_{n=1}^9 \epsilon_n P_n \right]}{q_{ref}}$$

where  $P$  is the pressure measured on the boattail and  $\epsilon$  is the projected boattail area weighting factor for the pressure orifice (see Fig. 8 for  $\epsilon$  values used).

### 2.3.5 Precision of Measurements

Uncertainties (bands which include 95 percent of the calibration data) of the basic experimental parameters were estimated from repeat calibrations of the instrumentation. Uncertainties of the instrumentation systems were estimated from repeat calibrations against secondary standards that have traceability to NBS. The uncertainties were combined using the Taylor series method of error propagation (Ref. 10) to determine the precision of the principal experimental parameters presented in Table 1.

## 3.0 RESULTS AND DISCUSSION

Typical static-pressure distributions obtained in the annular jet tests are shown in Fig. 9. The annular nozzle inlet flow acceleration region ( $X < 0$ ), the acceleration and deceleration of flow near the afterbody shoulder ( $0 < X < 4$  in.), and the subsequent reacceleration along the sting ( $X > 4$  in.) to the free-stream Mach number is readily evident. Pressures obtained at different angular locations at the same axial position on the afterbody were generally within the estimated uncertainty of the measurements.

### 3.1 BOUNDARY-LAYER CONDITIONS

One of the major concerns in the annular jet tests was to obtain afterbody approach boundary layers similar to those obtained in the wind tunnel tests while maintaining minimum boundary-layer development along the annular nozzles. While unit Reynolds numbers in the annular jet tests ( $2.7 \times 10^6$  to  $4.6 \times 10^6$ ) spanned the range of wind tunnel conditions ( $3.6 \times 10^6$  to  $4.6 \times 10^6$ ), the portion of the forebody contained within the annular nozzles was only one-fourth to one-half the length of the short ( $L/D = 8.8$ ) wind tunnel model. Consequently, forebody boundary layers produced by natural development in the annular tunnels were approximately one-fourth to one-half as thick as boundary layers on the short wind tunnel model. Afterbody boundary-layer development was, therefore, augmented in the annular jet tests by (1) downstream translations of the centerbody, (2) addition of a roughness element to the forebody, or (3) a combination of (1) and (2).

Exit boundary layer thicknesses (Fig. 10) of the annular nozzles varied from about 0.1 in. for the 6-in. nozzle to about 0.3 in. for the 12-in. nozzle. Forebody boundary layers produced by natural development with maximum downstream translation of the afterbody (Fig. 11,  $X_{ref} = 7$  in.) were 0.25 to 0.3 in. thick as compared with the 0.4-in. thickness obtained on the short wind tunnel model. With the roughness element installed and the afterbody within 2 in. of the annular nozzle exit, forebody boundary-layer thicknesses were similar (Fig. 12) to those of the short wind tunnel model.

In terms of the power law velocity distribution,

$$\frac{Y}{\delta} = \left( \frac{v}{v_o} \right)^N$$

boundary layers produced on the wind tunnel model can be bracketed (Ref. 8) by  $N$  between 7 and 9. In the annular tunnels, naturally developed forebody boundary layers correspond to power law distributions with  $N$  ranging from 9 to 11 (Fig. 13a), whereas  $N$  between 5 and 9 brackets the boundary layers obtained with the roughness element installed (Fig. 13b).

In the wind tunnel tests, local afterbody Mach numbers obtained with the short forebody configuration ( $L/D = 8.8$ ) were a maximum of 2.8 percent greater than those obtained at the same location with the long forebody ( $L/D = 13.8$ ). Boundary-layer thicknesses produced with the long forebody were approximately twice as thick as those obtained with the short model (see, for example, Fig. 12). Therefore, it is reasonable to assume that boundary layer differences between the annular jet and wind tunnel tests with the short forebody indicated in Fig. 12 should have negligible effect on afterbody Mach number comparisons. As a result, the assessment of annular tunnel interference effects was made from comparisons of the annular tunnel data obtained with the roughness element installed and the wind tunnel data obtained with the short forebody model.

### 3.2 AFTERBODY FLOW CONDITIONS

Afterbody Mach number distributions obtained in the wind tunnel with the short forebody are shown in Fig. 14. The critical reference Mach number for the afterbody is 0.85 with maximum local Mach numbers occurring near the shoulder ( $1.2 \lesssim X_c \lesssim 2.2$ ).

Typical afterbody Mach number distributions obtained in the 6-in.-diam annular jet, which produced the most significant interference effects, is presented in Fig. 15. Data obtained with the roughness element installed and the afterbody located to provide forebody boundary layers similar to wind tunnel conditions produced Mach number distributions (Fig. 15a) which are similar to wind tunnel results (Fig. 14).

In the annular tunnel installations, axial pressure gradients are introduced into the flow field by effects of boundary-layer growth and shear layer development on the free-jet boundary. Some indication of axial pressure gradient effects on afterbody flow conditions is evident from results (Fig. 15b) obtained without the roughness element installed. With subcritical reference Mach numbers, model translations corresponding to  $X_{ref}$  from -1 to 7 in. produced maximum Mach number variations of  $\pm 3$  percent. With supercritical reference

Mach numbers, interaction of the supersonic region of the afterbody flow field with the developing shear layer on the free-jet boundary made the flow in the shoulder region very sensitive to model position. At both subcritical and supercritical reference conditions, downstream movement of the model produced interactions that decelerated the flow in the shoulder region while accelerating the flow near the juncture of the afterbody and the jet simulator sting ( $X_c > 2.5$  in.).

Deviations of local afterbody Mach numbers obtained in the annular jet installations from corresponding wind tunnel results are presented in Fig. 16. Annular jet data used in the comparisons were obtained with the roughness element installed and with the reference orifice positioned from 0 to 3 in. downstream of the annular nozzle exit station. With reference Mach numbers up to 0.94, maximum Mach number deviations ranged from about  $\pm 3$  percent with the 12-in. annular nozzle, -1 to +5 percent with the 8-in. annular nozzle, and from -3 to +7 percent with the 6-in. annular nozzle. There is a general trend in all of the annular tunnel results which indicates interference effects that tend to accelerate flow adjacent to the afterbody in the shoulder region. Upstream and downstream of the shoulder, annular tunnel interference decelerates the afterbody flow relative to conventional wind tunnel results.

Also shown in Fig. 16c are local afterbody Mach numbers obtained in the 12-in. annular nozzle with a reference Mach number of 0.98, which, intuitively, should have experienced very significant interference effects. In the shoulder region, significant (12-percent) interference effects were, in fact, produced. However, upstream and downstream of the shoulder, afterbody Mach numbers were within  $\pm 2$  percent of wind tunnel results. Furthermore, a portion of the discrepancy in the shoulder region may be attributable to the large gradients in pressure at reference Mach numbers near unity (Fig. 8) which significantly increases the uncertainty in the wind tunnel data interpolations.

Afterbody shoulder region flow accelerations induced by the annular streams generally resulted in boattail pressure drag coefficients that were greater than wind tunnel values (Fig. 17). Maximum drag coefficient differences ranged from 0.016 with the 12-in. nozzle to 0.060 with the 6-in. nozzle. Maximum differences were produced at reference Mach numbers near the critical value.

### 3.3 IMPLICATION OF THE RESULTS WITH RESPECT TO ENGINE TESTING

While the data obtained in the subsonic annular tunnel show larger interferences than are desirable for precise evaluation of external aerodynamic phenomena, tests which are concerned with engine exhaust nozzle operation may not be significantly affected. For example, it should be possible to obtain good subsonic annular tunnel evaluations of engines

equipped with BIDE exhaust nozzles (e.g., Fig. 1) if the auxiliary inlets are upstream of the boattail shoulder where the major tunnel interference effects occur. With properly tailored boundary-layer conditions, flow into the auxiliary inlets, inlet drag, and internal flow conditions obtained in the annular tunnel should be quite representative of interference-free performance. The major discrepancy should occur on the boattail where annular tunnel induced flow accelerations will increase the boattail pressure drag coefficients depending on the extent and angle of the boattail and the relative annular tunnel size.

Engines equipped with internal-external expansion plug nozzles (e.g., Fig. 1) should also be amenable to subsonic annular tunnel evaluations if they have relatively short, low boattail angle shrouds for the internal expansion region. In this case, the engine exhaust/external flow interactions which affect plug surface pressures should be well represented by annular tunnel results. However, the relatively high boattail angles associated with external expansion plug nozzles may preclude annular tunnel evaluation since tunnel-induced flow accelerations may significantly alter the engine exhaust/external flow interaction region particularly in the vicinity of the shroud exit.

#### 4.0 CONCLUSIONS

Aerodynamic interference on a representative axisymmetric afterbody boattail model was evaluated by comparison of data obtained in a relatively large wind tunnel and in annular jets to determine the feasibility of conducting turbine engine/external flow interaction tests in limited annular air streams. The 4-in.-diam afterbody model was tested in an 8- by 6-ft porous wall wind tunnel and in 6-, 8-, and 12-in.-diam annular jet nozzles.

Comparison of afterbody Mach number distributions and the boattail pressure drag coefficients obtained in the annular jets with wind tunnel results obtained with similar boattail approach Mach numbers and boundary-layer thicknesses leads to the following conclusions:

1. Annular jet interactions tend to accelerate the flow in the vicinity of the afterbody shoulder. Upstream and downstream of the shoulder, annular tunnel interference decelerates the flow relative to wind tunnel results.
2. With boattail approach Mach numbers between 0.49 and 0.94, local Mach numbers obtained with the annular nozzles differed from wind tunnel results by a maximum of  $\pm 3$  percent with the 12-in. nozzle, -1 to +5 percent with the 8-in. nozzle, and -3 to +7 percent with the 6-in. nozzle.
3. Local afterbody Mach numbers obtained in the 12-in. annular nozzle with a boattail approach Mach number of 0.98 were within  $\pm 2$  percent of wind



tunnel results upstream and downstream of the afterbody shoulder region. In the shoulder region, local Mach numbers from the annular tunnel ranged from -4 to +12 percent of wind tunnel results. However, a portion of this difference may be attributable to uncertainties in the interpolation of wind tunnel results which are significant near Mach 1.0.

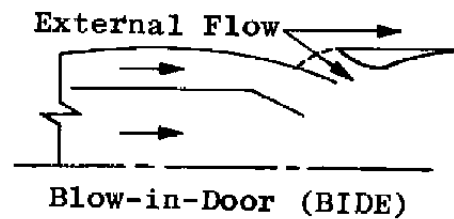
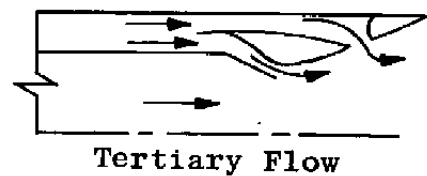
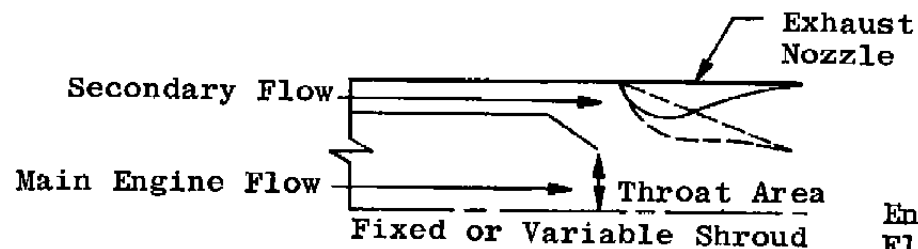
4. Boattail pressure drag coefficients obtained in the annular jets were generally greater than wind tunnel values. Maximum drag coefficient differences were obtained near the afterbody critical Mach number (0.85) and varied from 0.016 with the 12-in. nozzle to 0.060 with the 6-in. nozzle.

While the data obtained in the annular jets show larger interferences than are desirable for precise evaluation of external aerodynamic phenomena, the results indicate that the annular jet test technique may have potential application for engine exhaust/external interaction studies.

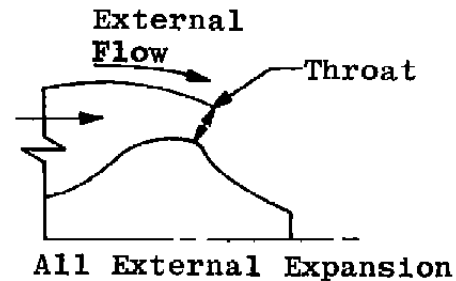
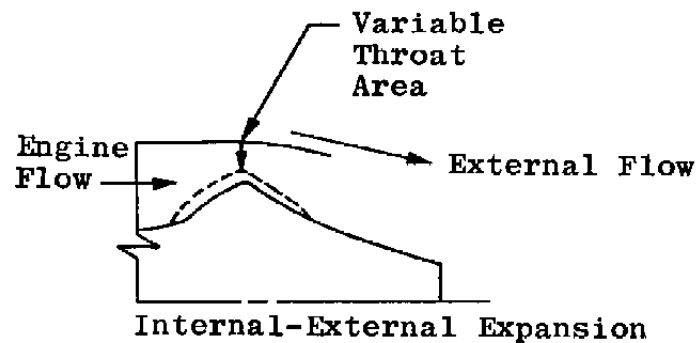
## REFERENCES

1. Migdal, D. and Horgan, J. J. "Thrust Nozzles for Supersonic Transport Aircraft." Journal of Engineering for Power, Transactions ASME, Series A, Vol. 86, No. 2, 1964, pp. 97-104.
2. Laughrey, J. A. "Calculation of the Performance of Installed Exhaust Nozzles on Supersonic Aircraft". AIAA 5th Propulsion Joint Specialist Conference, Paper No. 69-428, June 9-13, 1969.
3. Wehofer, S. and Matz, R. J. "Turbine Engine Exhaust Nozzle Performance with Nonuniform Inlet Flow." AEDC-TR-75-82 (ADA014261), August 1975.
4. Peters, C. E. "Annular Nozzles for Missile Base Flow Testing." AEDC-TN-60-62 (AD236195), May 1960.
5. Wilson, R. L. and Peters, T. "Recirculation of Turbopump Exhaust Gases about the Base of a 0.107-Scale Model of the Series E Atlas with Subsonic External Flows." AEDC-TN-59-75 (AD313455), November 1959.
6. Gillard, T. J. and Dawson, J. G., Jr. "An Investigation of Base Recirculation with a 1/10-Scale Atlas Missile Model in a Mach 2.0 External Flow Field." AEDC-TN-60-158 (AD318267L), August 1960.

7. Bergman, D. "Effects of Engine Exhaust Flow on Boattail Drag." Journal of Aircraft, Vol. 8, No. 6, June 1971, pp. 434-439.
8. Shrewsbury, G. D. "Effect of Boattail Juncture Shape on Pressure Drag Coefficients of Isolated Afterbodies." NASA TM-X-1517, March 1968.
9. ASME Research Committee on Fluid Meters. Fluid Meters-Their Theory and Application. The American Society of Mechanical Engineers, New York, 1971 (Sixth Edition).
10. Abernethy, R. B., et al., Pratt and Whitney Aircraft, and Thompson, J. W., Jr., ARO, Inc. "Handbook Uncertainty in Gas Turbine Measurements." AEDC-TR-73-5 (AD755356), February 1973.

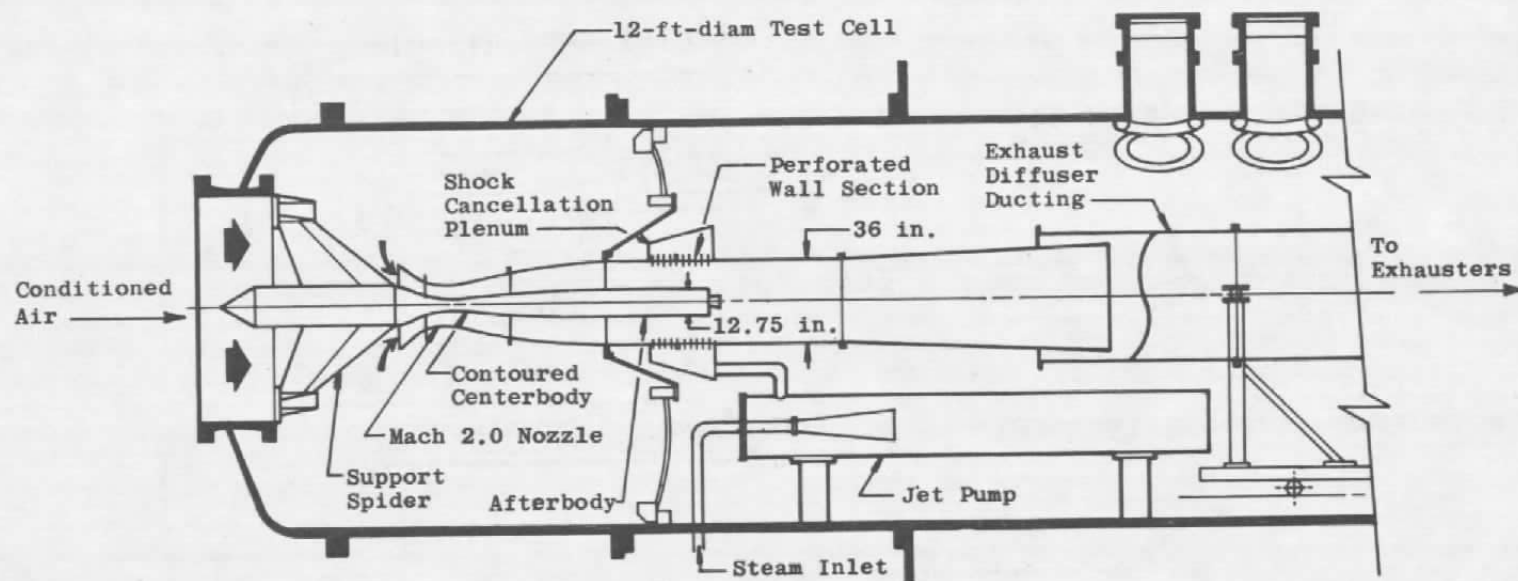


Ejectors



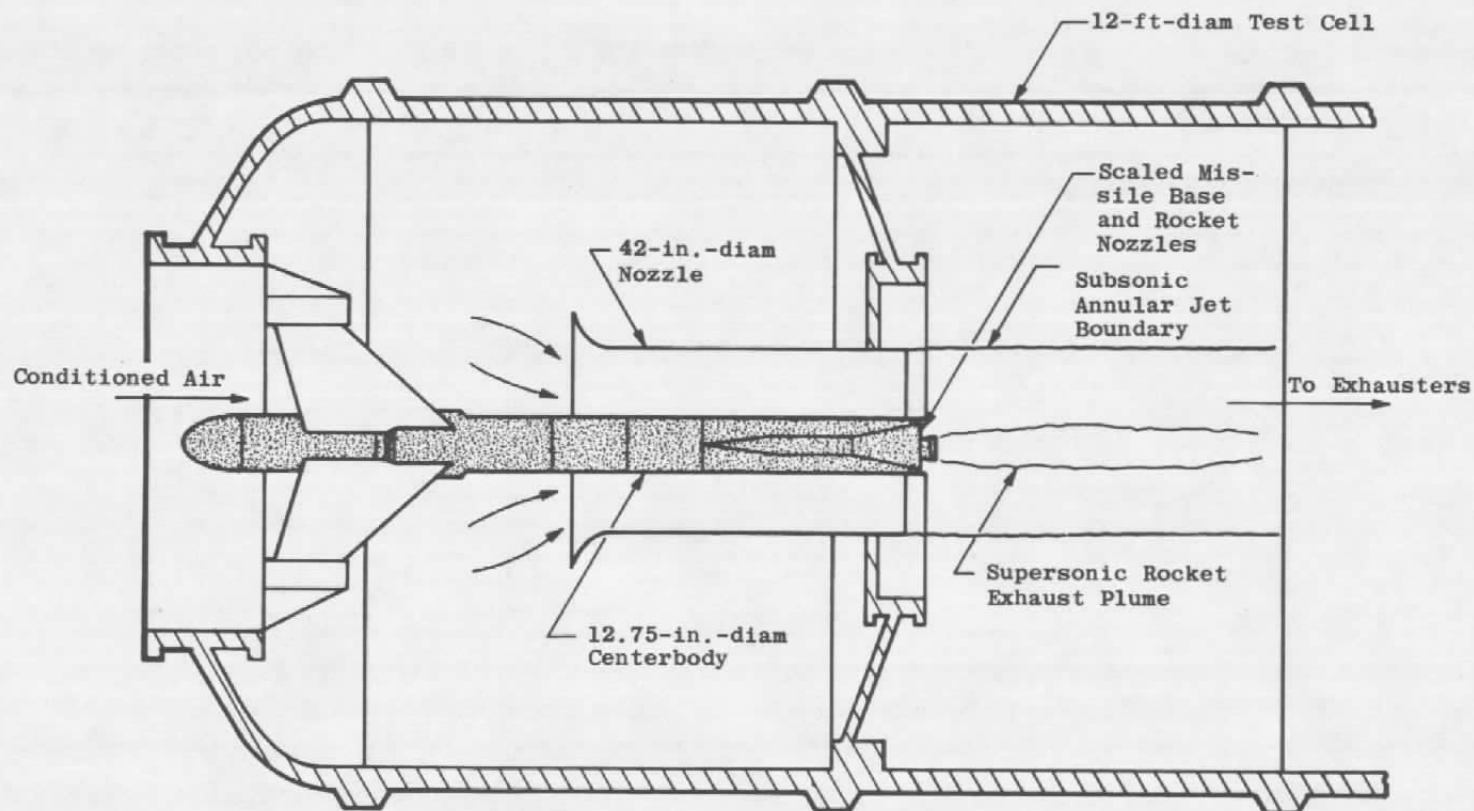
Plug Nozzles

Figure 1. Typical turbine engine exhaust nozzle configurations.



a. Supersonic external flow (Ref. 6)

Figure 2. Annular jet test installations for missile model base flow investigations.



b. Subsonic external flow (Ref. 5)  
Figure 2. Concluded.

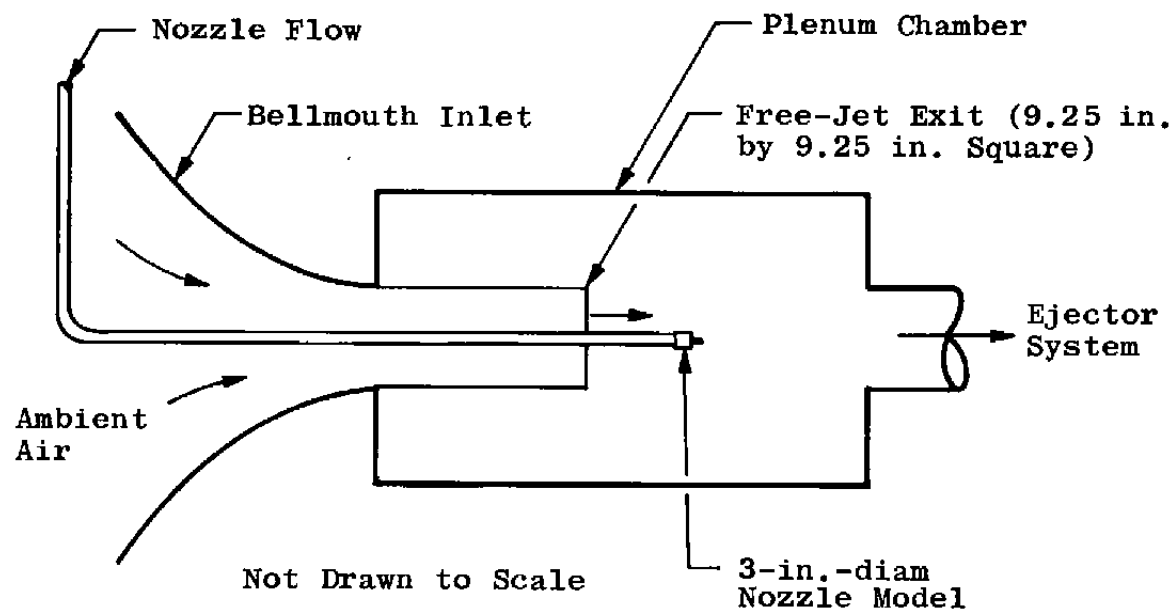
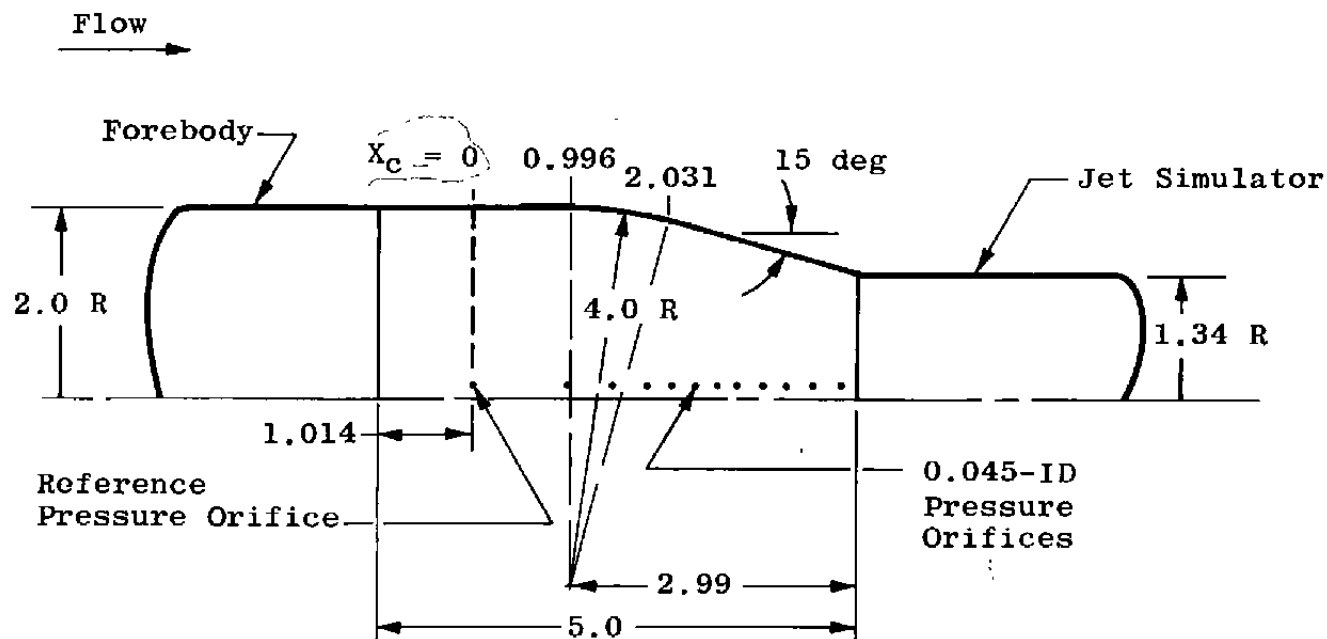


Figure 3. Subsonic annular jet tunnel for afterbody model investigations (from Ref. 7).



- Notes:
1. All Dimensions in Inches
  2. As-Built Coordinates Are Within  $\pm 0.002$  in. of Values Shown

Figure 4. Details of the afterbody model.

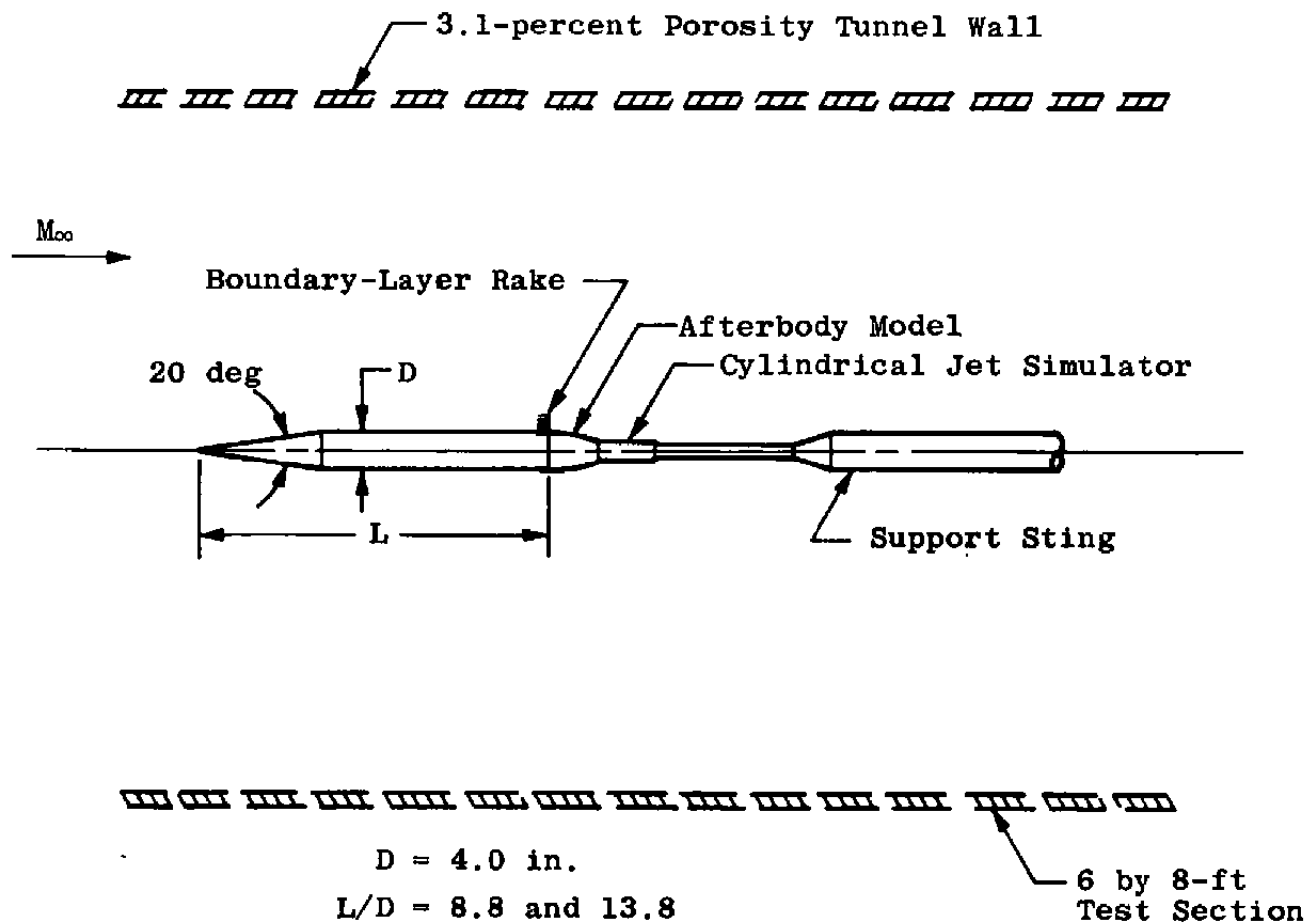


Figure 5. Wind tunnel installation (Ref. 8).



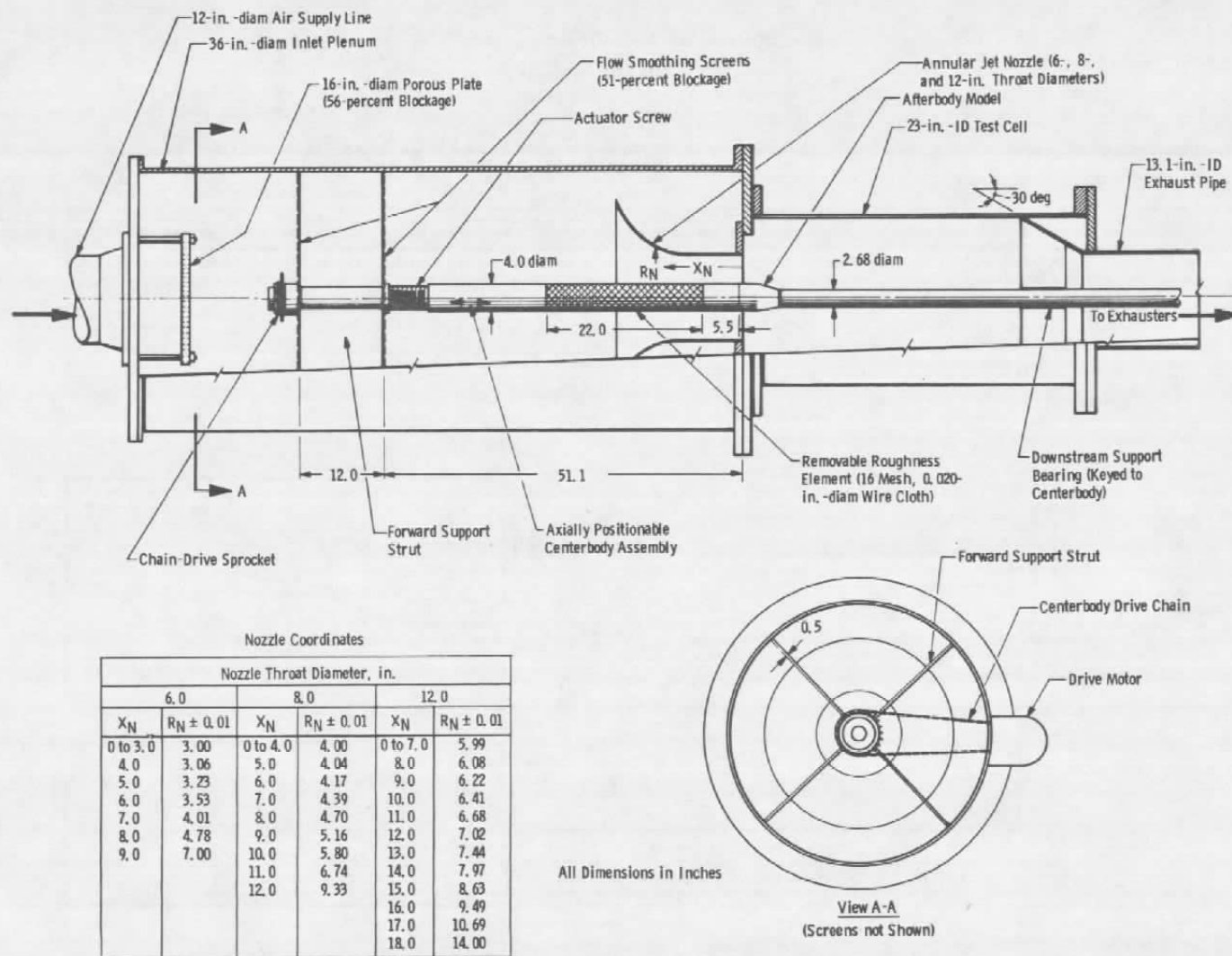
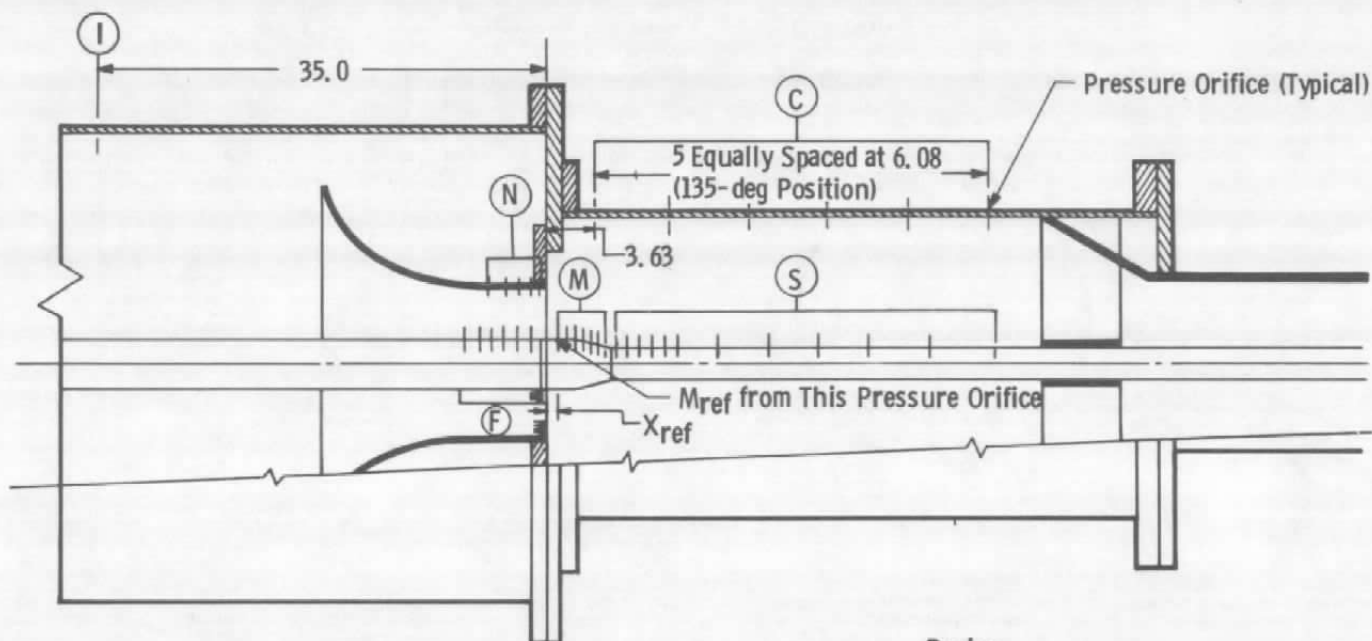


Figure 6. Annular jet installation.



Number of Sensors

Region	I	N	F	M	S	C
Total Pressure	---	7	8	---	---	---
Static Pressure	3	10	7	17	16	7
Total Temperature	3	---	---	---	---	---

## Region Designation

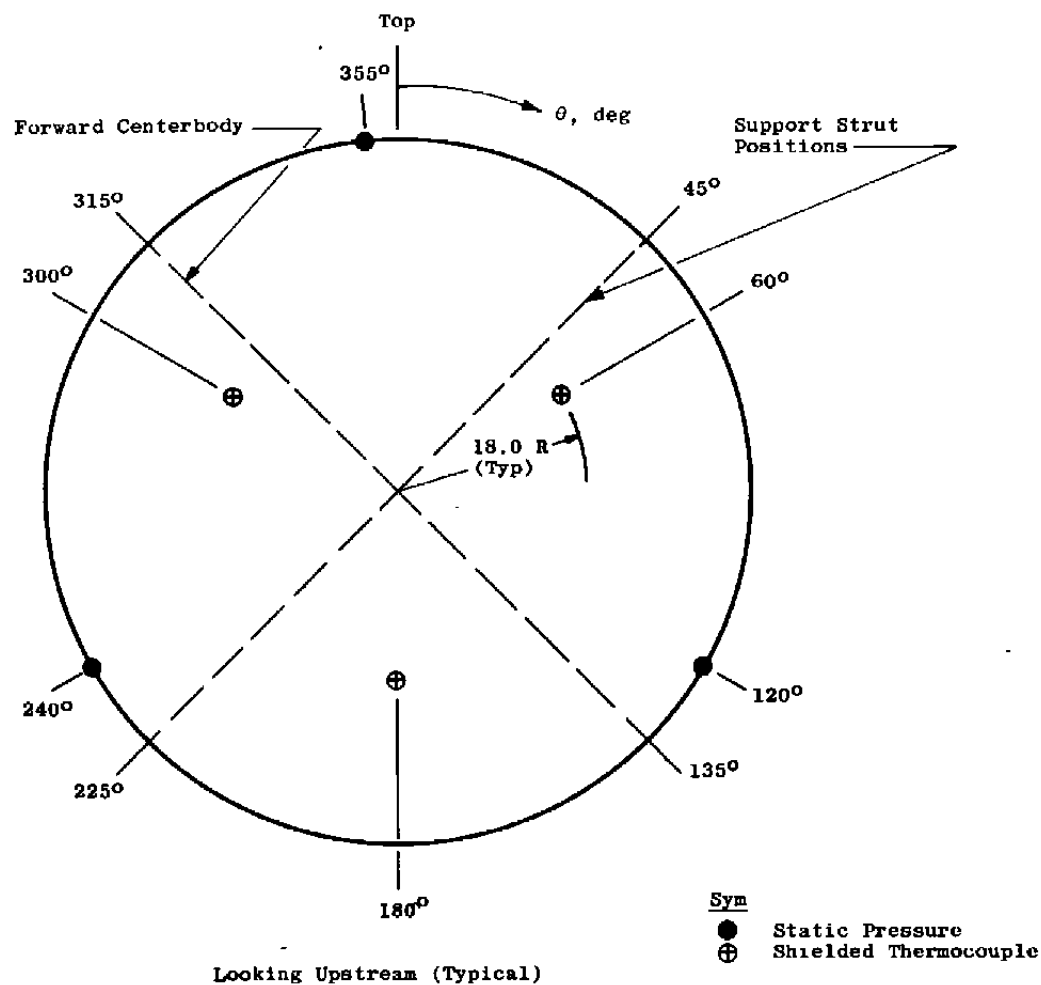
## Location

I	Inlet Plenum
N	Nozzle
F	Foreward of Afterbody Model
M	Afterbody Model
S	Plume Simulator
C	Cell Wall

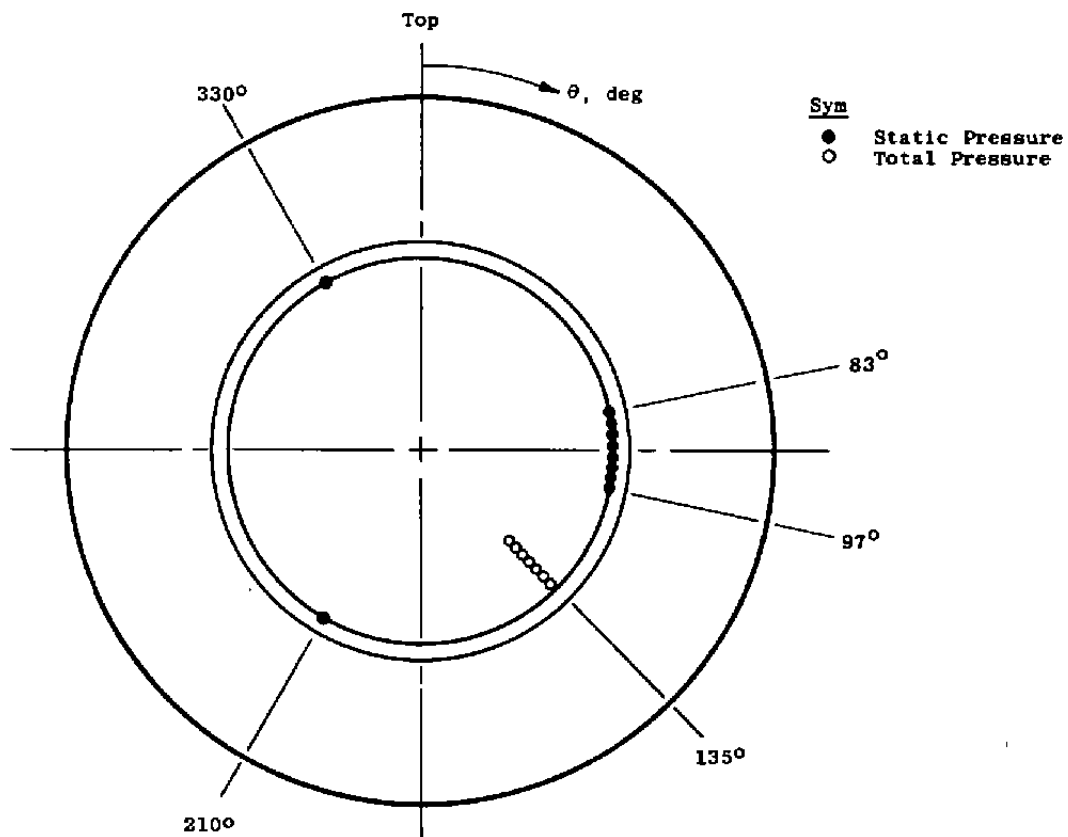
- Notes: 1.  $X_C = 0$  Corresponds to Reference Pressure Orifice Location on Afterbody Model (See Fig. 4)  
 2. All Dimensions in Inches

## a. Region locations

Figure 7. Annular jet instrumentation.



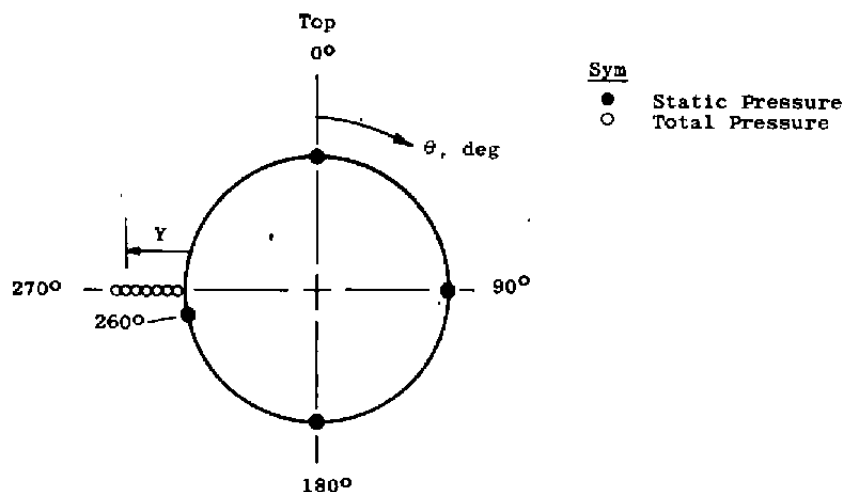
b. Inlet plenum (Region I)  
Figure 7. Continued.



Total Pressures
$\theta = 135$ deg, $X_n = 0.25$ in.
$Y = 0.03, 0.10, 0.17, 0.24, 0.3, 0.5, \text{ and } 0.77$ in.

Static Pressures	
$\theta$ , deg	$X_n$ , in.
83	0.12
85	0.25
87	0.50
89	0.75
91	1.0
93	1.5
95	3.0
97	4.5
210	0.25
330	0.25

c. Nozzle (Region N)  
Figure 7. Continued.



Region F	
Static Pressures	
θ, deg	X <sub>C</sub> , in.
90	-7.0
	-6.0
	-5.0
	-4.0
	-3.0
	-2.0
260	-2.0
Total Pressures	
θ = 270 deg, X <sub>C</sub> = -2.0 in.	
Y = 0.04, 0.10, 0.17, 0.24, 0.30, 0.50, and 0.72 in.	

Region M	
Static Pressures	
θ, deg	X <sub>C</sub> , in.
90	0
	1.0
	1.488
	1.819
	2.084
	2.309
	2.541
	3.036
	3.297
	3.572
	3.861
0	0
0	2.541
0	3.861
180	1.488
180	2.541
180	3.861

Region S	
Static Pressures	
θ, deg	X <sub>C</sub> , in.
90	4.26
	4.51
	5.0
	6.0
	7.0
	8.0
	9.0
	10.0
	11.0
	12.0
	13.0
	14.0
	19.0
	24.0
	29.0
	34.0

d. Centerbody (Regions F, M, and S)  
Figure 7. Concluded.

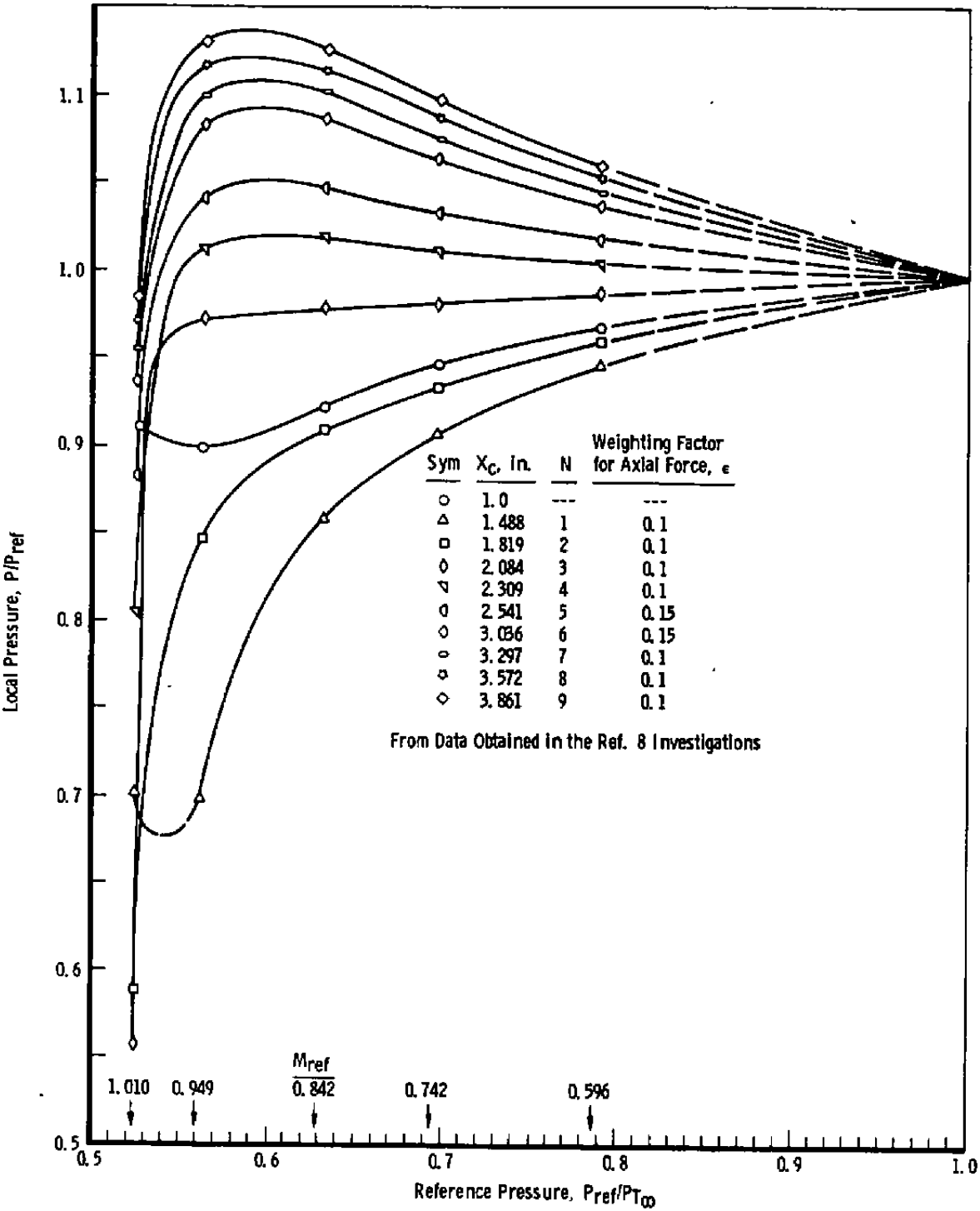
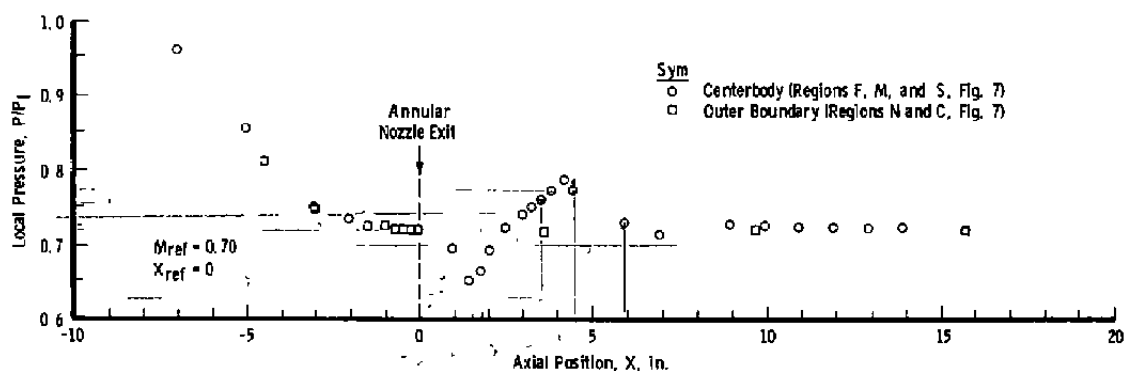
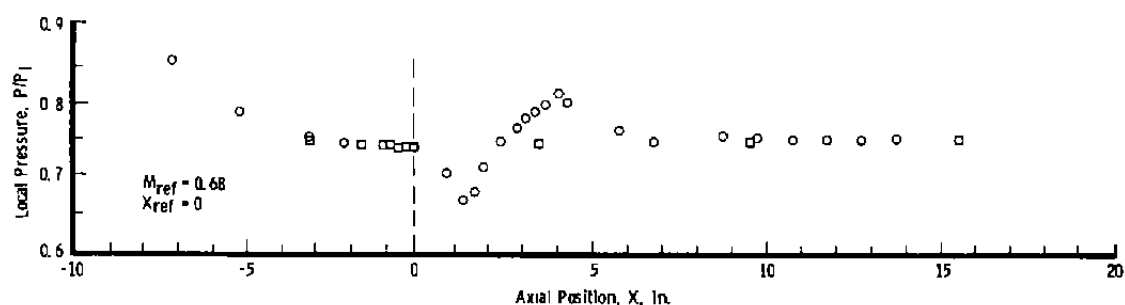


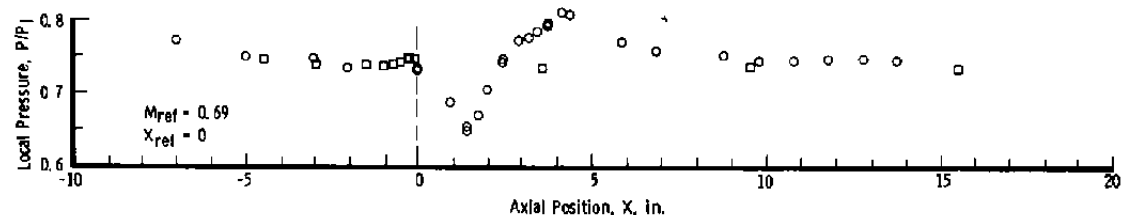
Figure 8. Variation of local afterbody pressures obtained in the wind tunnel with the reference pressure.



a. 6-in.-diam annular jet nozzle



b. 8-in.-diam annular jet nozzle



c. 12-in.-diam annular jet nozzle

Figure 9. Typical static pressure distributions obtained in the annular jet installations.

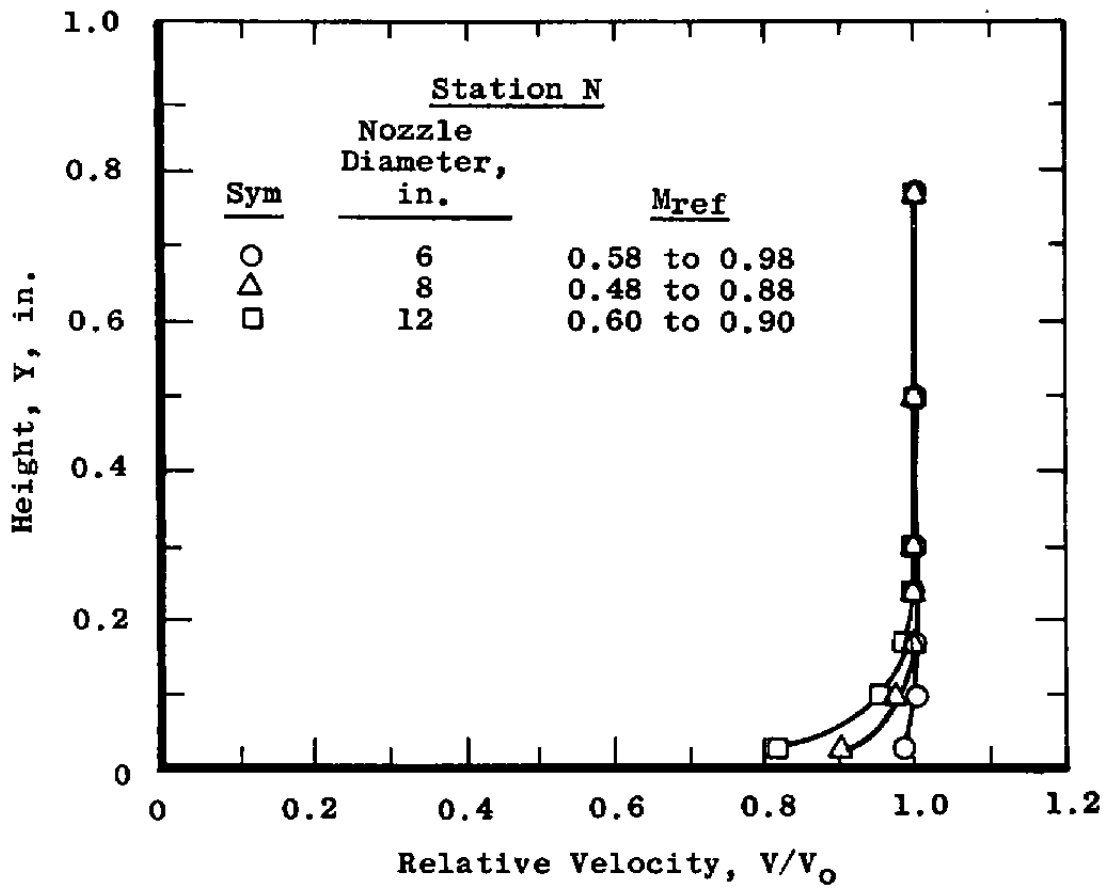
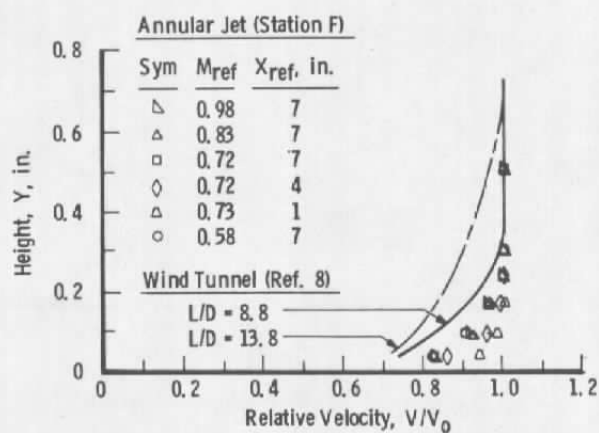
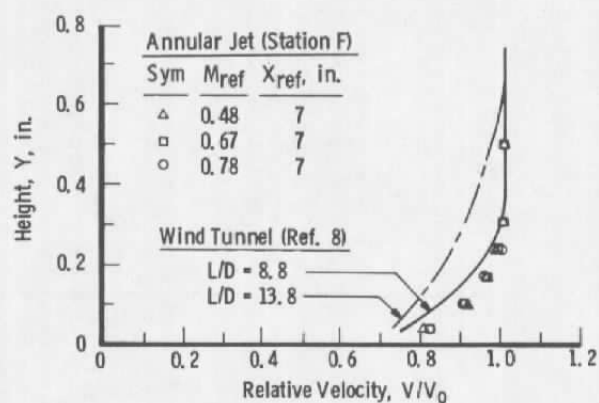


Figure 10. Typical annular jet nozzle exit boundary-layer velocity profiles.

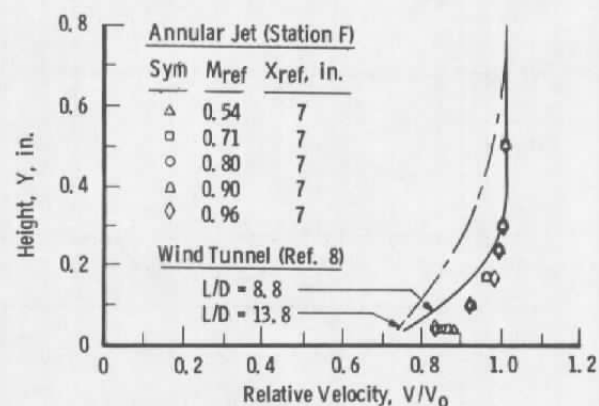




a. 6-in.-diam annular jet nozzle

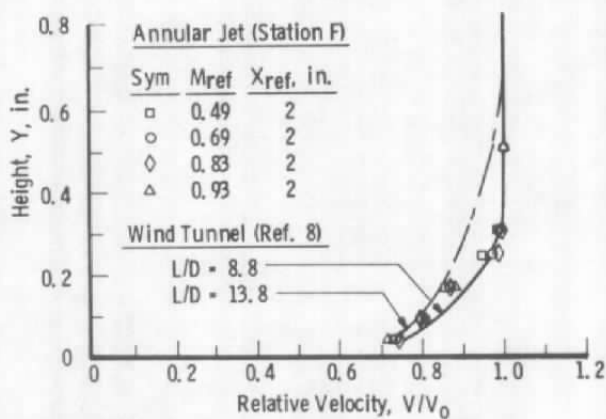


b. 8-in.-diam annular jet nozzle

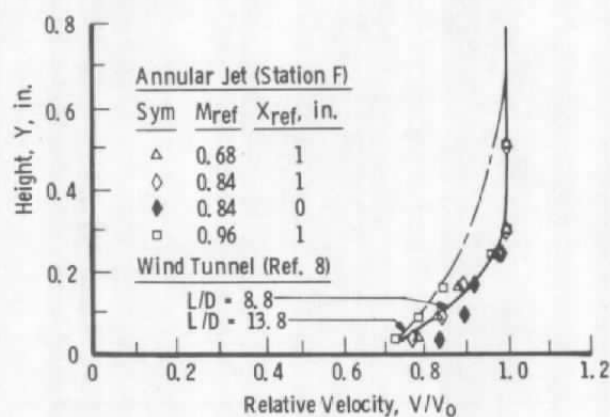


c. 12-in.-diam annular jet nozzle

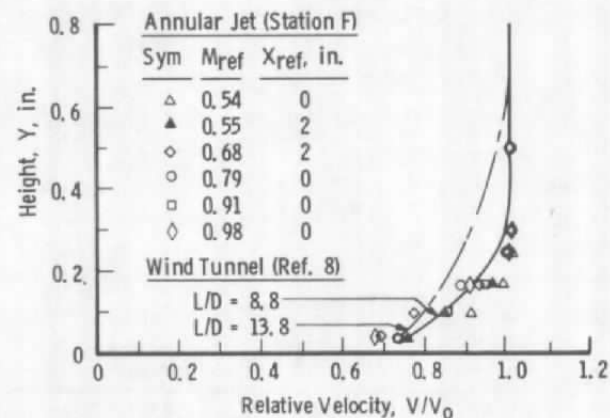
Figure 11. Comparison of afterbody boundary layers obtained in the wind tunnel and in the annular tunnels with natural development.



a. 6-in.-diam annular jet nozzle



b. 8-in.-diam annular jet nozzle



c. 12-in.-diam annular jet nozzle

Figure 12. Comparison of afterbody boundary layers obtained in the wind tunnel and in the annular tunnels with the roughness element installed.

Sym	Nozzle Annular
○	6 in.
□	8 in.
△	12 in.

Note: . N between 7 and 9 for Wind Tunnel Model with  
L/D = 8.8 Forebody

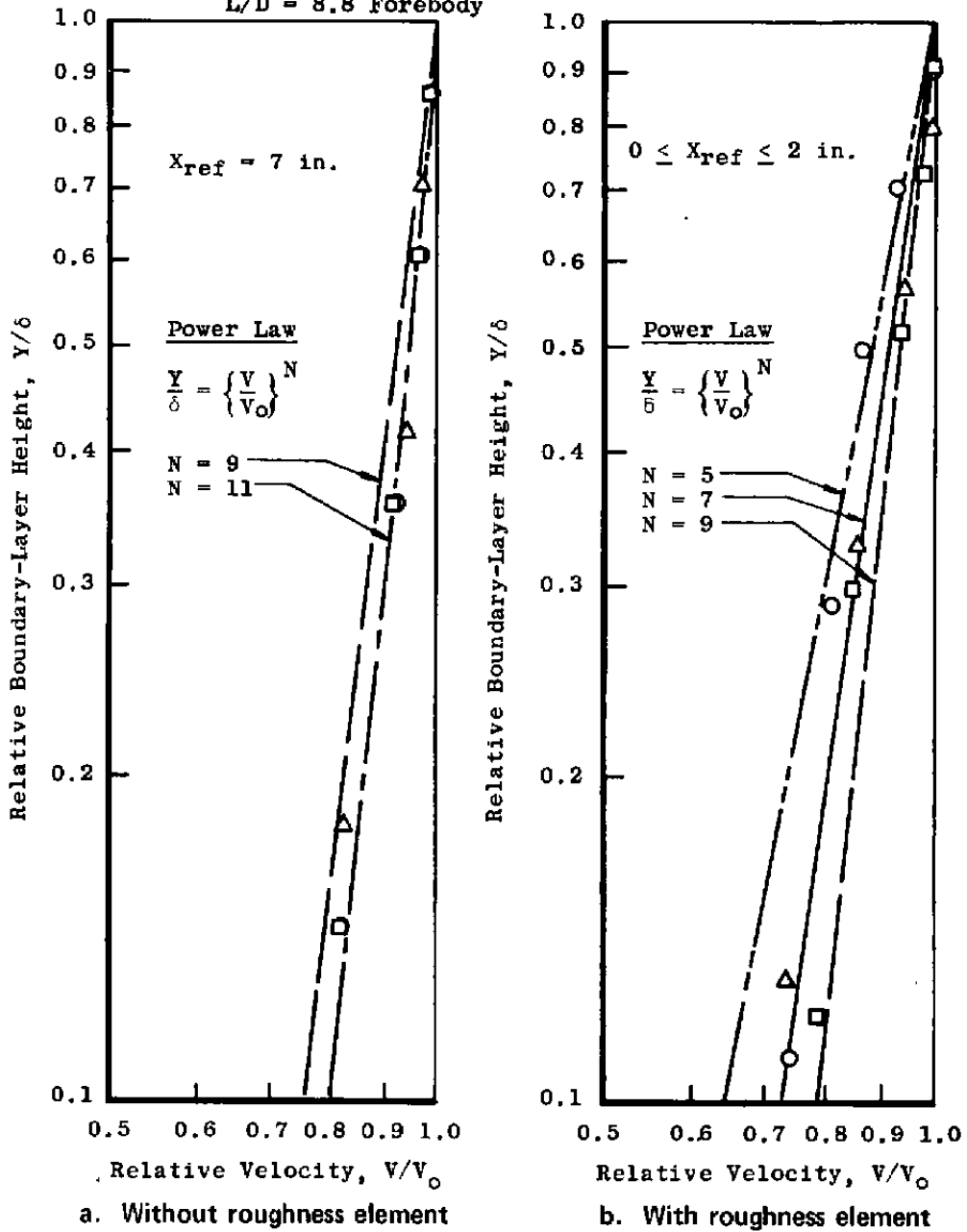


Figure 13. Comparison of boundary-layer velocity profiles obtained in the annular jets with power law representations.

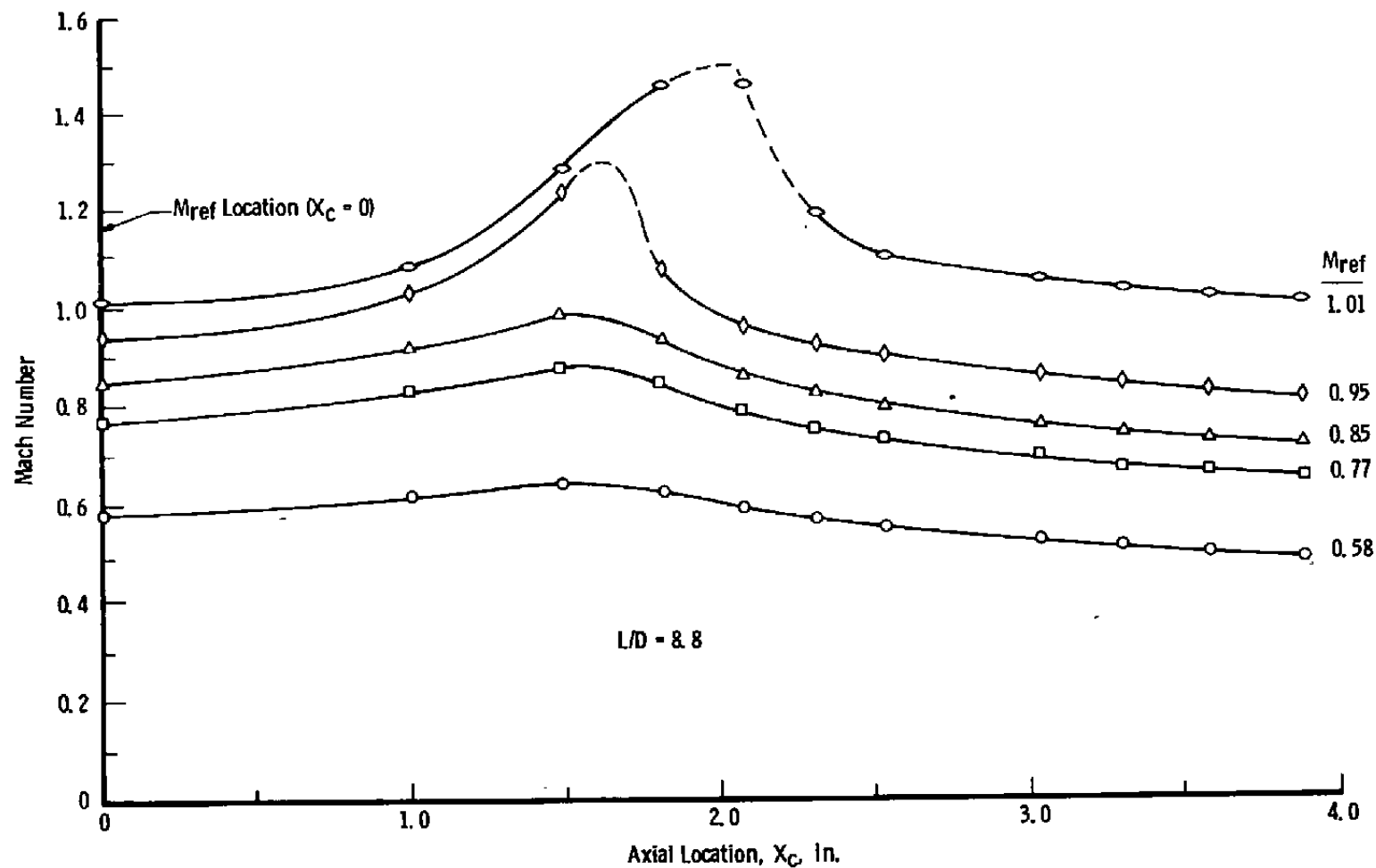
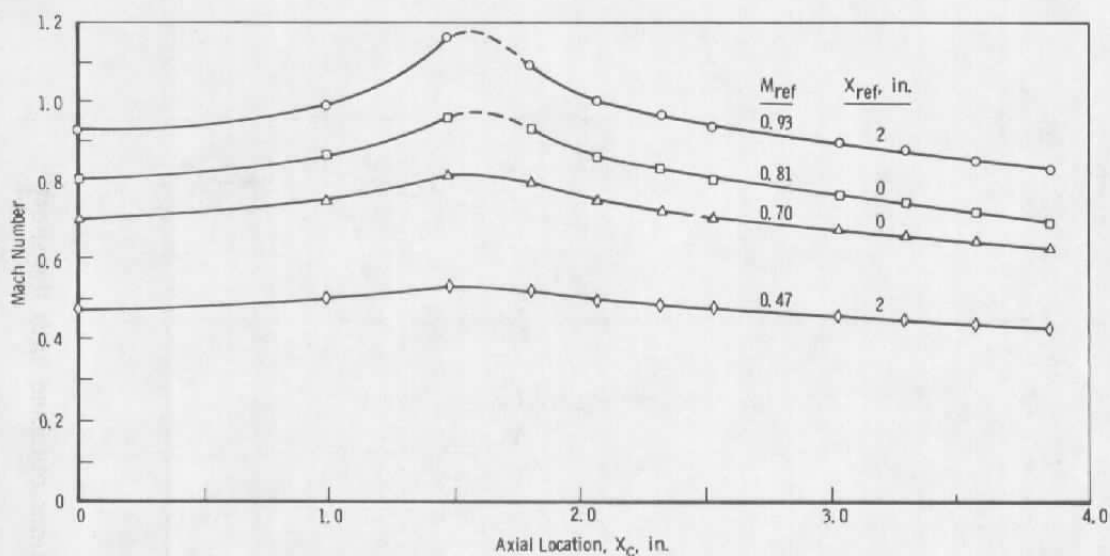
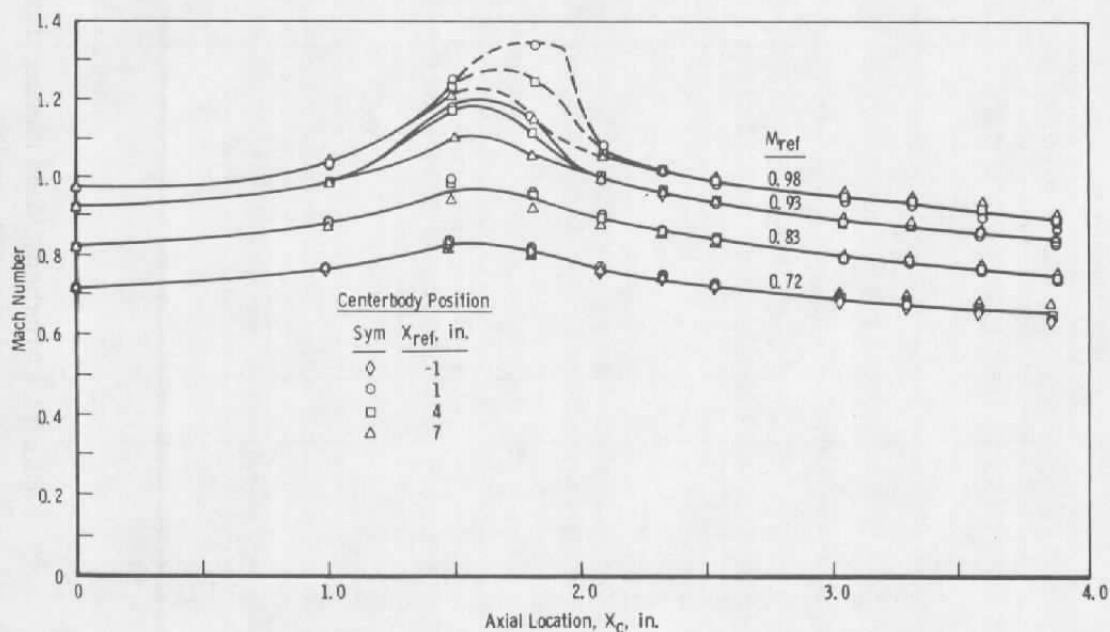


Figure 14. Afterbody Mach number distributions obtained with the short wind tunnel models.

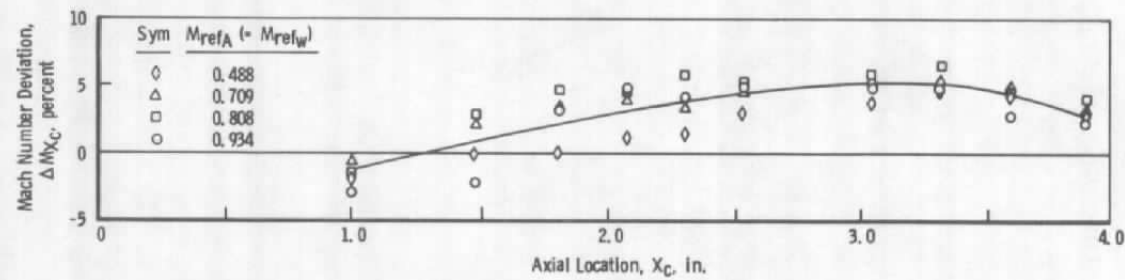


a. With roughness element installed

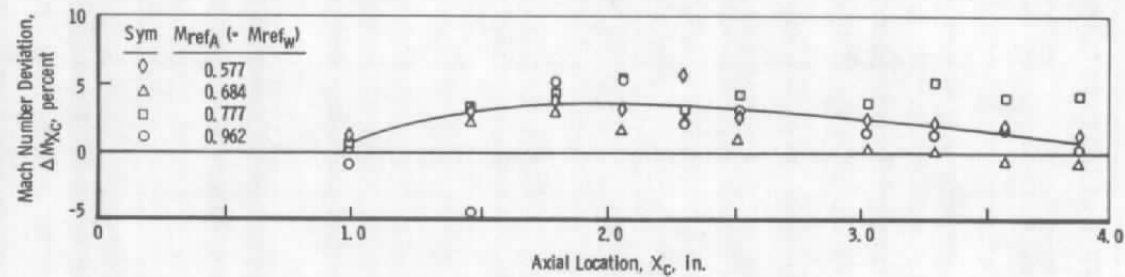


b. With natural boundary-layer development

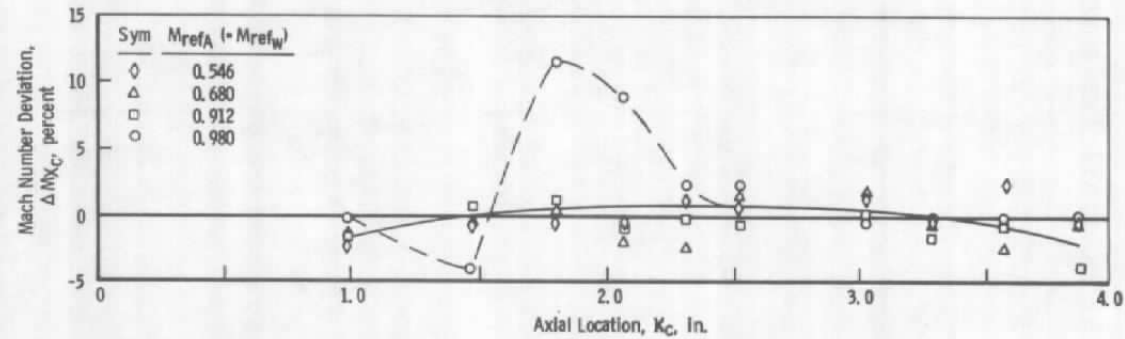
Figure 15. Typical afterbody Mach number distributions obtained in the 6-in. annular tunnel.



a. 6-in.-diam annular jet nozzle



b. 8-in.-diam annular jet nozzle



c. 12-in.-diam annular jet nozzle

Figure 16. Deviation of afterbody Mach number distributions obtained in the annular jet nozzles with surface roughness from wind tunnel results.

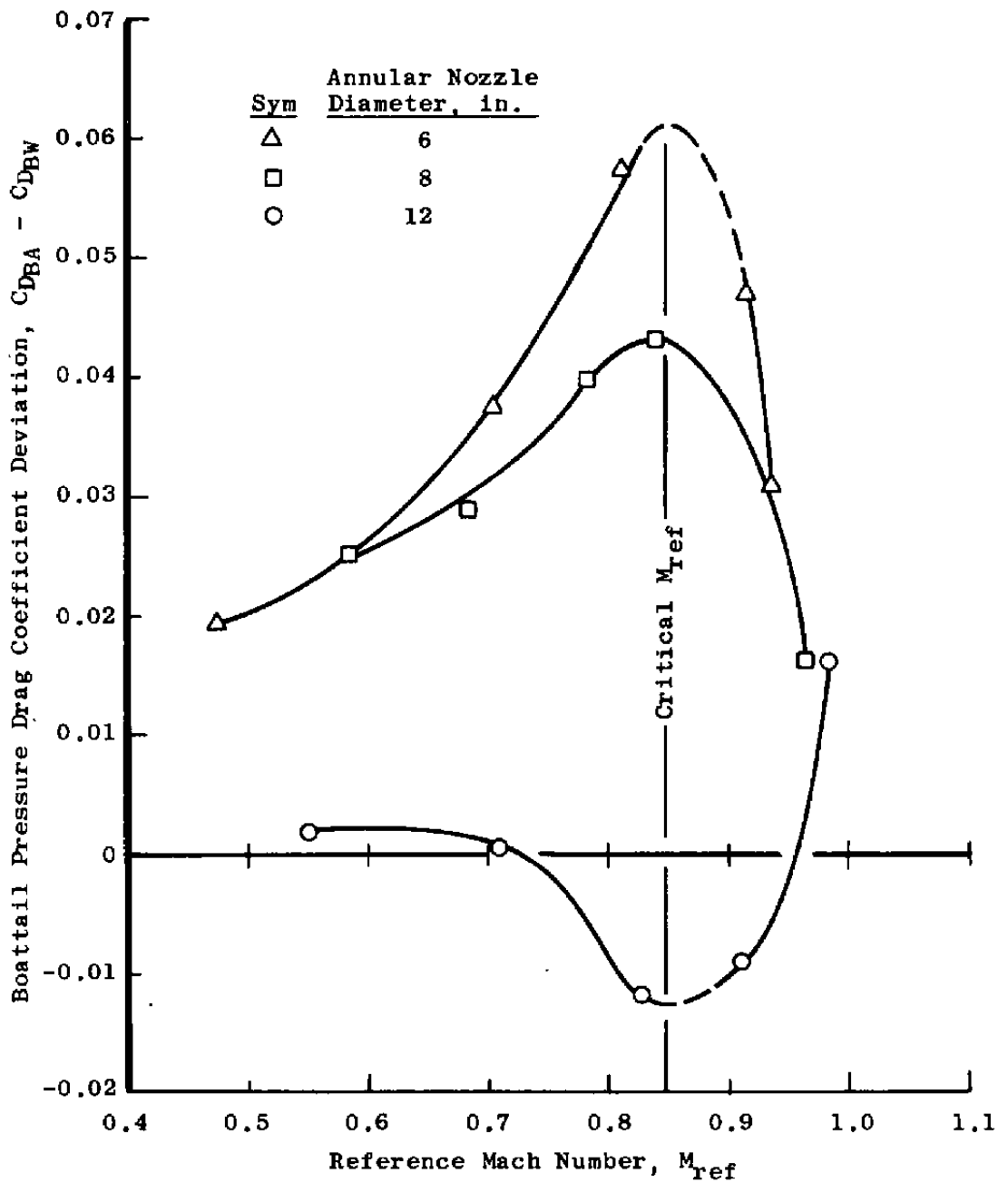


Figure 17. Deviation of boattail pressure drag coefficients obtained in the annular jet streams from the wind tunnel results.

Table 1. Estimated Uncertainty in the Principal Annular Nozzle Test Parameters

Nominal Test Conditions			Estimated Uncertainty					
$M_{ref}$	$P_{Tref}$ psia	$T_{TI}$ °F	$\pm \Delta P$ Percent of Reading	$\pm \Delta T$ °F	$\pm \Delta X_{ref}$ in.	$\pm \Delta(P/P_T)$	$\pm \Delta M$	$\pm \Delta C_{DB}$
0.5	13.0	60	0.6	5	0.1	0.0072	0.013	0.0200
0.6						0.0067	0.011	0.0140
0.7						0.0061	0.010	0.0103
0.8						0.0056	0.009	0.0080
0.9						0.0050	0.008	0.0062
1.0						0.0045	0.007	0.0046



## NOMENCLATURE

$C_{DB}$	Boattail pressure drag coefficient (Eq. (2))
$D$	Diameter, in.
$L$	Forebody length, in.
$M$	Mach number
$N$	Exponent in boundary-layer power law velocity distribution
$P$	Static pressure, psia
$P_t$	Annular nozzle inlet plenum pressure, psia
$P_{ref}$	Static pressure from afterbody reference orifice, psia
$P_T$	Total pressure, psia
$q$	Dynamic pressure, psia
$R$	Radial position, in.
$T_{T1}$	Total temperature, °F
$V$	Velocity, ft/sec
$X$	Axial position, in.
$X_c$	Axial position of pressure orifices relative to the afterbody reference pressure orifice, in.
$X_{ref}$	Axial position of afterbody reference pressure orifice relative to annular nozzle exit plane, in.
$Y$	Position normal to adjacent surface, in.
$\Delta M_{xc}$	Percent difference between local afterbody Mach number obtained in the annular jet and in the wind tunnel

$\delta$	Boundary-layer thickness, i.e., point where local velocity is 99.5 percent of free-stream velocity, in.
$\epsilon$	Boattail pressure orifice weighting factor in the pressure drag determination
$\theta$	Angular position, deg

## SUBSCRIPTS

A	Annular tunnel
n	Boattail pressure orifice index
o	Free stream adjacent to boundary layer
w	Wind tunnel
$\infty$	Wind tunnel plenum